Received: 23 May 2024 | Revised: 25 July 2024 | Accepted: 29 August 2024 | Published online: 12 September 2024

RESEARCH ARTICLE

Journal of Optics and Photonics Research
2025, Vol. 2(2) 77–85
DOI: 10.47852/bonviewJOPR42023479

BON VIEW PUBLISHING

The Output Field of Curved Waveguides with a Cross-Section of Alternating Hollow and Dielectric Layers

Zion Menachem[1,*]

[1]*Department of Electrical Engineering, Sami Shamoon College of Engineering, Israel*

Abstract: The aim of this study is to investigate the effects on the output field of curved (helical and toroidal) waveguides having a rectangular cross-section made up of seven alternating hollow and dielectric layers. In this study, we will generalize the specific problem of a waveguide with the above cross-section from a straight waveguide to both helical and toroidal-shaped waveguides. We use a technique based on the inverse transforms of the Laplace and Fourier transforms for this purpose. This study clarifies how the cylinder radius and helix angle affect power transmission and output fields in this particular instance of a periodic cross-section. The findings hold true in the microwave and millimeter-wave domains and can be helpful in applications involving helical or toroidal waveguides with periodic arrays of alternating hollow and dielectric layers. The results are true in the microwave and millimeter-wave regimes and can find utility in applications using a periodic array with alternating hollow and dielectric layers in a helical or toroidal waveguide. According to the logical results we get in the output profiles, we can determine what are the logical parameters that should be taken before any experiment in the laboratory that we want to perform.

Keywords: wave propagation, helical and toroidal waveguides, helix angle, dielectric material, rectangular waveguide

1. Introduction

The literature on curved waveguides regards both optical waveguides (e.g., Marcatili and Schmeltzer [1]) and metallic waveguides (e.g., Marhic [2]), and are valid in the microwave regimes. The first researchers who were interested in bending waveguides for different applications were described in Marcatili and Schmeltzer [1], Marhic [2] and Miyagi et al. [3]. According to the theory of Marcatili and Schmeltzer [1], the bending is considered as a small disturbance. A mode-coupling analysis of a curved waveguide was proposed in Marhic [2]. An improved solution for $r/R \ll 1$ was offered in Miyagi et al. [3].

Many articles were published over time. We will provide some interesting examples of the applications in all kinds of fields, for example in structures based on periodic photonic crystals, in photonic integrated circuits, in photonic communication, and in other fields. Curved waveguides with laser beam were proposed in Wang et al. [4]. The huge curved waveguide's design based on a sunflower-graded photonic crystal was presented in Liu et al. [5]. The characterization of optical spot-size converter couplers was given in Qvotrup et al. [6]. The elastic wave propagation in rectangular waveguides was studied in Groth et al. [7]. Elastic-guided wave propagation in a helical waveguide was given in Melloni et al. [8]. A numerical method for computing the fields in curved rectangular waveguides was described in Rosa [9]. Arbitrary curved waveguide for the lattice photonic media was proposed in Krushynska et al. [10]. Propagation in a 3D waveguide with curved waveguide was proposed in Guennoc et al. [11]. Propagation that relates to Rayleigh wave and the influence on curved surfaces was given in Zhang et al. [12]. A broadband acoustic bend featuring homogeneously curved waveguides was introduced [13].

Articles that refer to periodic waveguide, periodic metal structures, and periodic metamaterials were published over time. We will give interesting examples of recently published publications. Acoustic solutions in a periodic waveguide were proposed in Sougleridis et al. [14]. A direct near-field observation of the conversion in periodic structure between waveguide modes and leaky modes was provided in Wu et al. [15]. Analysis of waveguide for periodic medium was presented in Darche et al. [16]. Periodic stub implementation with a plasmonic cavity waveguide was proposed in Tabatabaeian et al. [17]. Analysis of periodic waveguide with arbitrary shaped corrugation was proposed in Salem et al. [18]. Complex modes for periodic waveguide were proposed in Abdrabou and Lu [19]. Complex Bloch modes in optical chain waveguides were proposed Ghahremani and Shahabadi [20].

A numerical technique was presented for the propagation along a straight dielectric waveguide with an arbitrary cross-section in Menachem and Jerby [21]. An efficient technique to solve a periodic array in the case of a straight waveguide was proposed in Menachem [22]. An effective technique for resolving inhomogeneous problems with dielectric material

*Corresponding author: Zion Menachem, Department of Electrical Engineering, Sami Shamoon College of Engineering, Israel. Email: zionme@sce.ac.il

between the metal of curved waveguides and the hollow rectangle was introduced in Menachem [23].

This study aims to investigate the effects on the output field of curved waveguides with 7 alternating hollow and dielectric layers in the cross-section. The ω_ε function was proposed in Vladimirov [24] to solve inhomogeneous cross-section. In this study, we will generalize the method outlined in Menachem [22] from a straight waveguide to curved waveguides for the given periodic cross-section. For this purpose, we will use the method for curved waveguides [23] for the specific case of the periodic cross-section (Figure 1(c)).

2. Curved Waveguides with the Periodic Cross-Section

Figure 1(a) shows a rectangular helical waveguide in three-dimensional space ($\delta_p = 0.2$–1.0), and Figure 1(b) shows a rectangular toroidal waveguide on a two-dimensional plane ($\delta_p = 0$). Namely, the bending in Figure 1(b) refers to bending in the plane. On the other hand, the bending in Figure 1(a) refers to bending in three-dimensional space. The coordinate along the helix axis is denoted by ζ, and the cylinder radius is denoted by R.

From the deployment of the helix (Figure 1(d)), δ_p is the helix angle, $\varnothing_c$ is the planar and peripheral angle, where $0 \leq \varnothing_c \leq 2\pi$ and $\varnothing_c = (\zeta/R)\cos(\delta_p)$. From this, it can be seen that the radius of the cylinder of the helical waveguide (Figure 1(a)) depends on the three parameters ζ, δ_p, and $\varnothing_c$ according to the following relationship:

$$R = \frac{\zeta \cos(\delta_p)}{\phi_c} \tag{1}$$

Figure 1(c) shows the waveguide cross-section. This cross-section is an interesting structure of a periodic array. This cross-section of a periodic array has an intriguing structure. There are 7 alternating hollow and dielectric layers that make up the periodic cross-section. The layers 2, 4, and 6 are represented by the thicknesses d_1, d_2, and d_3, correspondingly. It is assumed in this study that $d_1 = d_2 = d_3 = d$. The dielectric material (ε_{r1}, ε_{r2}, ε_{r3}) of layers 2, 4, and 6 can be different. We suppose in this study that according to Figure 1(c), that L_1 = a/4, L_2 = a/2, and $L_3 = 3a/4$, respectively.

3. Generalization of the Periodic Cross-Section from a Straight Waveguide to a Curved Waveguide

The aim of this research is to investigate wave propagation along curved waveguides with periodic cross-sections. In this study, we will generalize the method introduced in Menachem [22] from a straight waveguide to curved waveguides for the specific periodic cross-section (Figure 1(c)).

Seven alternating hollow and dielectric layers make up the periodic array that makes up the cross-section under study. In this study, we will generalize the method introduced in Menachem [22] from a straight waveguide to curved waveguides for the specific periodic cross-section (Figure 1(c)). For this purpose, we will use the method in Menachem [23] for helical and toroidal waveguides for this specific case of the periodic cross-section (Figure 1(c)). The inverse Laplace and Fourier transforms constitute the basis of the procedure. Salzer proposed the inverse Laplace transform in the s-plane [25, 26]. The computer program was written using NAG subroutines (https://nag.com).

Figure 1

Schematic illustration of the rectangular cross-section waveguides: (a) the helical waveguide; (b) the toroidal waveguide; (c) the rectangular cross-section with 7 alternating hollow and dielectric layers; (d) deployment of the helix

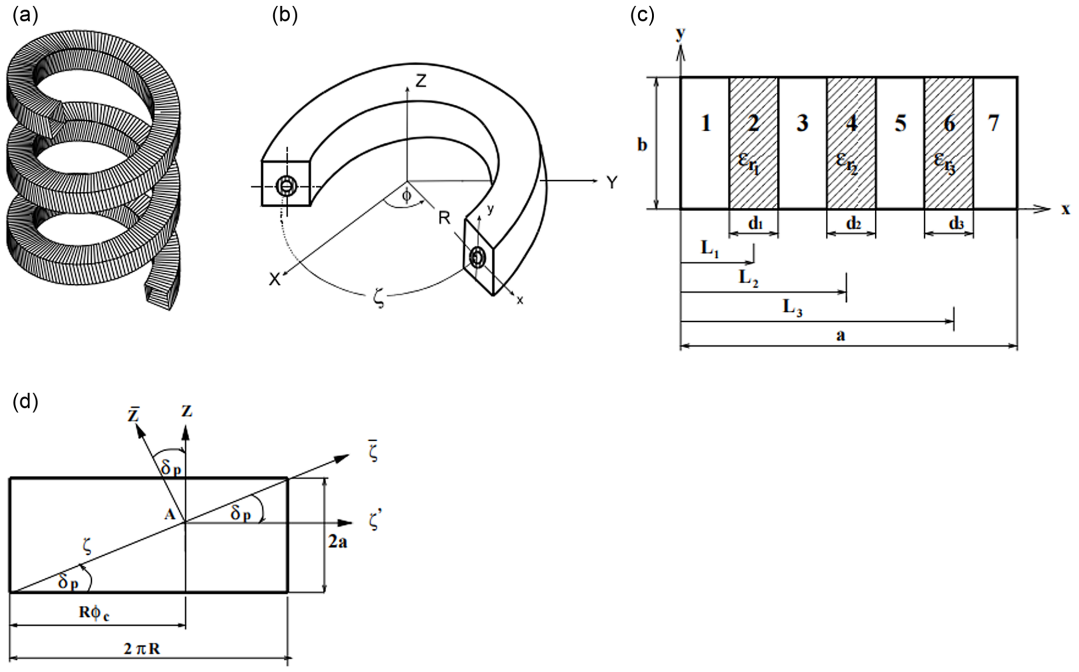

We must create precise phrases for each matrix element. The ω_ε function was proposed in Vladimirov [24] and is given by

$$\omega_\varepsilon(r) = C_\varepsilon \exp\left(-\frac{\varepsilon^2}{\varepsilon^2 - |r|^2}\right) \tag{2}$$

for $|r| > \varepsilon$, where C_ε is a constant, and $\int \omega_\varepsilon(r)\mathrm{d}r = 1$.

Figure 2 shows the proposed ω_ε function according to Equation (2) and according to Vladimirov [24]. The function (Equation (2)) is important to solve an inhomogeneous transition at the boundary between medium 1 to medium 2, between medium 2 to medium 3, and etc., as shown in Figure 1(c). The elements of the matrix are based on Equation (2) and are calculated by

$$\mathrm{g(n,m)} = \frac{1}{\mathrm{ab}}\{(I_1(x) + I_2(x) + I_3(x) + I_4(x) + I_5(x) + I_6(x) + I_7(x) + I_8(x) + I_9(x))dx\}\left\{\int_0^b \cos\left(\frac{m\pi y}{b}\right)dy\right\},$$

Where:

$$I_1(x) = g_{01}\int_{(0.5a-d_1-\varepsilon)/2}^{(0.5a+d_1+\varepsilon)/2} \exp\left(1 - \frac{\varepsilon^2}{\varepsilon^2 - [x-(0.5a-d_1+\varepsilon)/2]^2}\right)\cos\left(\frac{n\pi x}{a}\right),$$
$$I_2(x) = g_{01}\int_{(0.5a-d_1+\varepsilon)/2}^{(0.5a+d_1-\varepsilon)/2} \cos\left(\frac{n\pi x}{a}\right),$$
$$I_3(x) = g_{01}\int_{(0.5a+d_1-\varepsilon)/2}^{(0.5a+d_1+\varepsilon)/2} \exp\left(1 - \frac{\varepsilon^2}{\varepsilon^2 - [x-(0.5a+d_1-\varepsilon)/2]^2}\right)\cos\left(\frac{n\pi x}{a}\right),$$

$$I_4(x) = g_{02}\int_{(a-d_2-\varepsilon)/2}^{(a-d_2+\varepsilon)/2} \exp\left(1 - \frac{\varepsilon^2}{\varepsilon^2 - [x-(a-d_2+\varepsilon)/2]^2}\right)\cos\left(\frac{n\pi x}{a}\right),$$
$$I_5(x) = g_{02}\int_{(a-d_2+\varepsilon)/2}^{(a+d_2-\varepsilon)/2} \cos\left(\frac{n\pi x}{a}\right),$$
$$I_6(x) = g_{02}\int_{(a+d_2-\varepsilon)/2}^{(a+d_2+\varepsilon)/2} \exp\left(1 - \frac{\varepsilon^2}{\varepsilon^2 - [x-(a+d_2-\varepsilon)/2]^2}\right)\cos\left(\frac{n\pi x}{a}\right),$$
$$I_7(x) = g_{03}\int_{(1.5a-d_3-\varepsilon)/2}^{(1.5a-d_3+\varepsilon)/2} \exp\left(1 - \frac{\varepsilon^2}{\varepsilon^2 - [x-((3a/2)-d_3+\varepsilon)/2]^2}\right)\cos\left(\frac{n\pi x}{a}\right),$$
$$I_8(x) = g_{03}\int_{(1.5a-d_3+\varepsilon)/2}^{(1.5a+d_3-\varepsilon)/2} \cos\left(\frac{n\pi x}{a}\right),$$
$$I_9(x) = g_{03}\int_{(1.5a+d_3-\varepsilon)/2}^{(1.5a+d_3+\varepsilon)/2} \exp\left(1 - \frac{\varepsilon^2}{\varepsilon^2 - [x-((3a/2)+d_3-\varepsilon)/2]^2}\right)\cos\left(\frac{n\pi x}{a}\right), \tag{3}$$

Figure 2
The ω_ε function used for solving the inhomogeneous problem of the cross-section described in Figure 1(c)

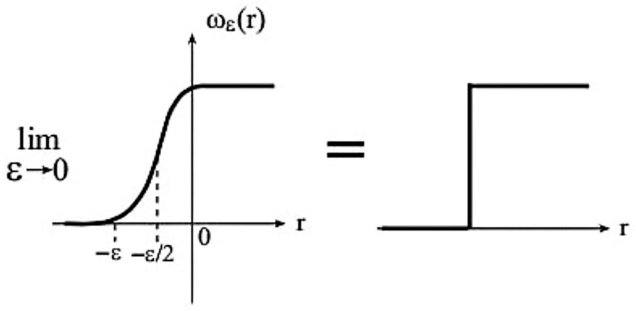

where $\varepsilon = a/50$. The matrix G is given by the following relation

$$\overline{g}(n,m)(n',m') = g_{n-n',m-m'}, \tag{4}$$

and this is a special matrix.

4. Numerical Results

The comparison of our model to the known analytical method [27] is shown in Appendix A.

Several examples are shown in this section to examine the effect of curved waveguides on the output power transmission and the field for TE_{10} mode. The following examples are demonstrated for $\zeta = 0.15$ m and where $a = b = 20$ mm.

Figure 3 shows the influence of the bending (1/R) for different helix angles ($\delta_p = 0.0,\ 0.2,\ 0.4,\ 0.6,\ 0.8,\ 1.0$) on the output power transmission in normalized units, where $\zeta = 0.15$ m, $a = b = 20$ mm, $\varepsilon_{r1} = \varepsilon_{r2} = \varepsilon_{r3} = 9$, $L_1 = a/4 = 5$ mm, $L_2 = a/2 = 10$ mm, and $L_3 = 3a/4 = 15$ mm, where the thickness of each of the three dielectric layers is $d = a/8 = 2.5$ mm. The results show the following. First, for a given value of R, the output power transmission is high for large values of δ_p. As the δ_p decreases, the output power transmission decreases as well. This indicates that increasing the helix angle can lead to improve the output power transmission through the helical waveguide. Second, for a given value of δ_p, the output power transmission is high for large values of R. Conversely, as the R decreases, the output power transmission also decreases. This suggests that increasing the cylinder radius can enhance the output power transmission through the helical waveguide. These results enable us to find the parameters of δ_p and R to obtain improved the output results of the output power transmission.

The following examples refer to the input wave profile TE_{10} mode and demonstrate the behavior of the profiles of the output field of the helical waveguide. From the results of Figure 3 we take the curve for $\delta_p = 1$. The output field for the given cross-section is displayed in Figures 4(a–e), 5(a–e), and 6(a–e) for $\delta_p = 1$, $\zeta = 0.15$ m, and where $a = b = 20$ mm.

Figure 4(a–d) demonstrate the output field for four values of the radius of the cylinder, $R = 53$ mm, $R = 44$ mm, $R = 38$ mm, and

Figure 3
The influence of bending (1/*R*) for different helix angles ($\delta_p = 0.0, 0.2, 0.4, 0.6, 0.8, 1.0$) on the output power transmission, where $\zeta = 0.15$ m, $a = b = 20$ mm, $\varepsilon_{r1} = \varepsilon_{r2} = \varepsilon_{r3} = 9$, $L_1 = a/4 = 5$ mm, $L_2 = a/2 = 10$ mm, $L_3 = 3a/4 = 15$ mm, where the thickness of each of the three dielectric layers is $d = a/8 = 2.5$ mm

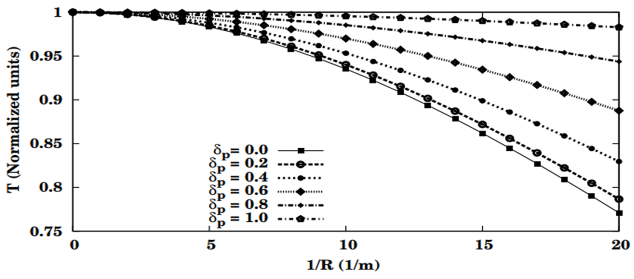

Figure 4

The results for TE_{10} mode for four values of R: (a) $R = 53$ mm; (b) $R = 44$ mm; (c) $R = 38$ mm; and (d) $R = 33$ mm for the periodic cross-section given in Figure 1(c). The other parameters are $d = a/6 = 3.33$ mm, $\varepsilon_{r1} = \varepsilon_{r2} = \varepsilon_{r3} = 7$, $L_1 = a/4 = 5$ mm, $L_2 = a/2 = 10$ mm, and $L_3 = 3a/4 = 15$ mm; (e) the output field for the results (a)–(d) for $R = 53$ mm, $R = 44$ mm, $R = 38$ mm, and $R = 33$ mm, where $y = 0.5$ b and for the x-axis

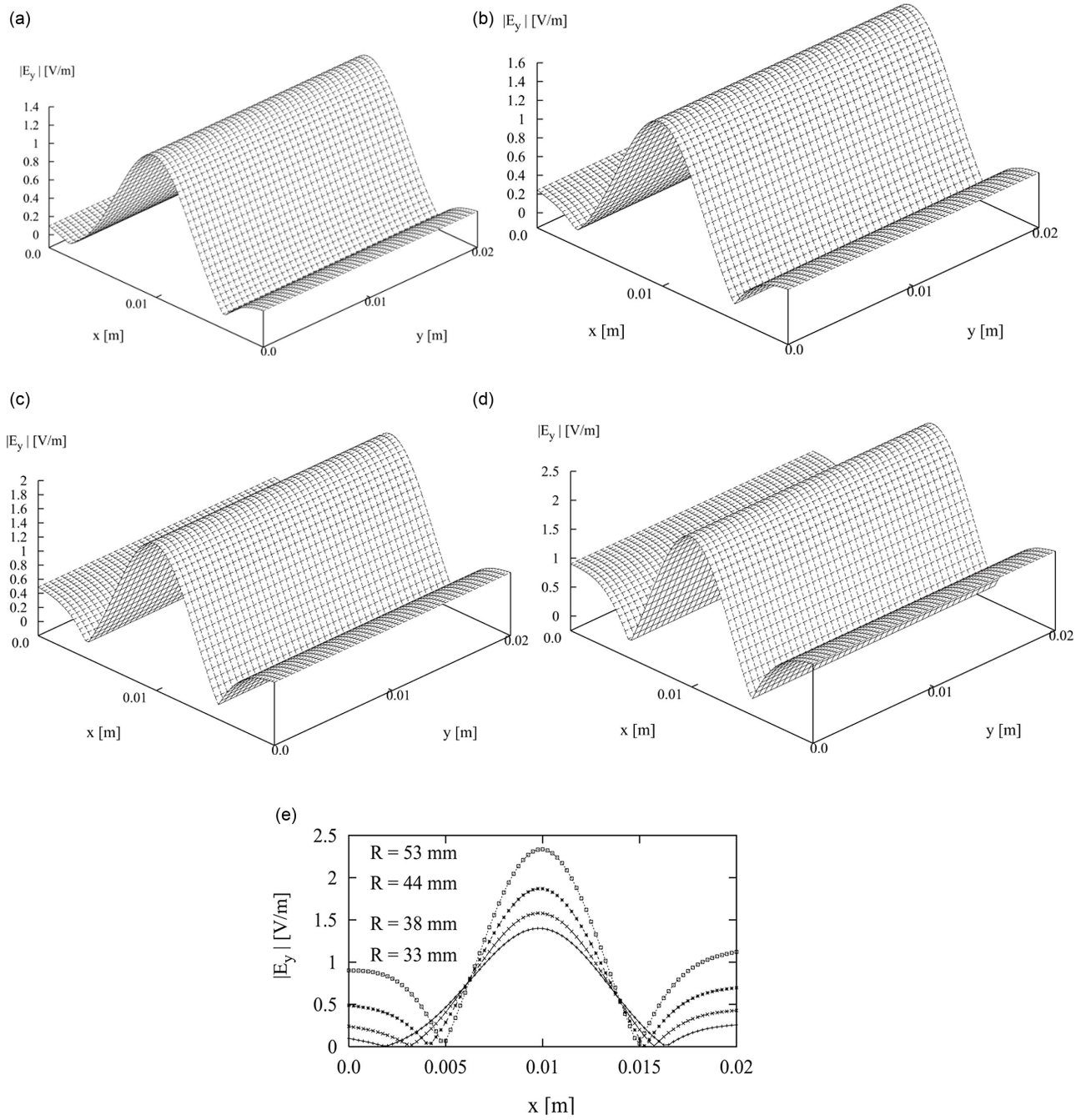

$R = 33$ mm, respectively. The thickness of each of the three dielectric layers is $d = a/6 = 3.33$ mm, $\varepsilon_{r1} = \varepsilon_{r2} = \varepsilon_{r3} = 7$, $L_1 = a/4 = 5$ mm, $L_2 = a/2 = 10$ mm, and $L_3 = 3a/4 = 15$ mm. The output field for the results of Figure 4(a–d) is displayed in Figure 4(e) for $R = 53$ mm, $R = 44$ mm, $R = 38$ mm, and $R = 33$ mm, where $y = 0.5$ b and for the x-axis.

Figure 5(a–d) demonstrate the output field for four values of the radius of the cylinder, $R = 53$ mm, $R = 38$ mm, $R = 29$ mm, and $R = 27$ mm, respectively. The thickness of each of the three dielectric layers is $d = a/7 = 2.86$ mm, $\varepsilon_{r1} = \varepsilon_{r2} = \varepsilon_{r3} = 10$, $L_1 = a/4 = 5$ mm, $L_2 = a/2 = 10$ mm, and $L_3 = 3a/4 = 15$ mm. The output field for the results of Figure 5(a–d) is displayed in Figure 5(e) for $R = 53$ mm, $R = 38$ mm, $R = 29$ mm, and $R = 27$ mm, where $y = 0.5$ b and for the x-axis.

The behavior of the output results of Figure 5(a–e) is changed significantly in relation to the results of Figure 4(a–e), through the

Figure 5
The results for TE_{10} mode for four values of R: (a) $R = 53$ mm; (b) $R = 38$ mm; (c) $R = 29$ mm; and (d) $R = 27$ mm and cross-section given in Figure 1(c). The other parameters are $d = a/7 = 2.86$ mm, $\varepsilon_{r1} = \varepsilon_{r2} = \varepsilon_{r3} = 10$, $L_1 = a/4 = 5$ mm, $L_2 = a/2 = 10$ mm, and $L_3 = 3a/4 = 15$ mm; (e) the output field for the results (a)–(d) for $R = 53$ mm, $R = 38$ mm, $R = 29$ mm, and $R = 27$ mm, where $y = 0.5\ b$

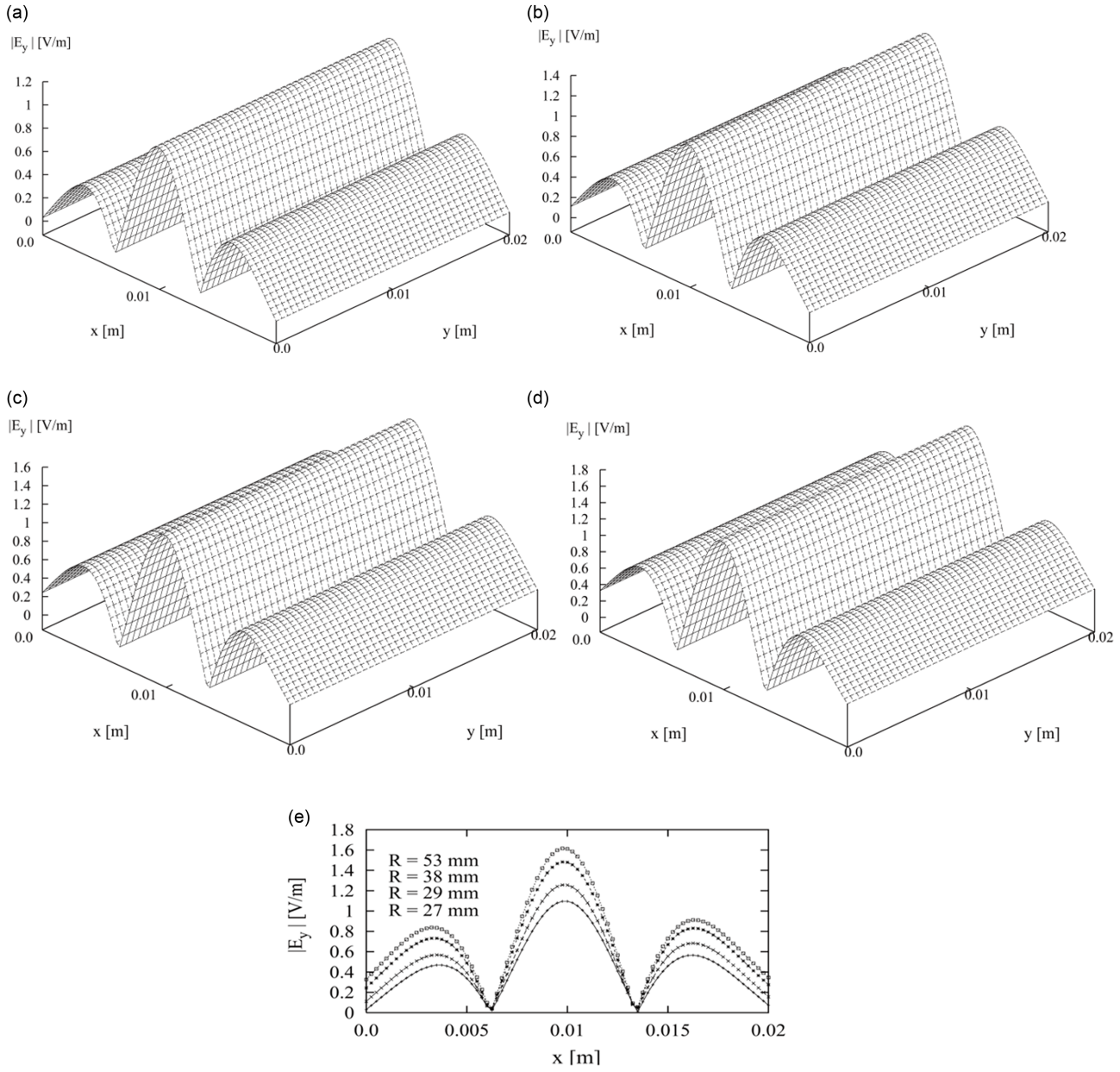

change of the thickness of each of the three dielectric layers from $d = a/6 = 3.33$ mm to $d = a/7 = 2.86$ mm and by increasing of ε_r from $\varepsilon_r = 7$ to $\varepsilon_r = 10$. By changing only the radius of the cylinder, we can see from the results of Figures 4(a–e) and 5(a–e) that the field amplitude is greater when the radius of the cylinder is greater and that the width of the output profile is narrower.

The output field for each of the four-cylinder radius values is shown in Figure 6(a–d), $R = 53$ mm, $R = 38$ mm, $R = 29$ mm, and $R = 27$ mm, respectively. The thickness of each of the three dielectric layers is $d = a/8 = 2.5$ mm, $\varepsilon_{r1} = \varepsilon_{r3} = 8$, $\varepsilon_{r2} = 9$, $L_1 = a/4 = 5$ mm, $L_2 = a/2 = 10$ mm, and $L_3 = 3a/4 = 15$ mm. Note that in this example, the value of ε_{r2} is different from the value of ε_{r1} and ε_{r3}. The output field for the results of Figure 6(a–d) is displayed in Figure 6(e) for $R = 53$ mm, $R = 38$ mm, $R = 29$ mm, and $R = 27$ mm, where $y = 0.5\ b$ and for the x-axis.

The behavior of the output results of Figure 6(a–e) is changed significantly in relation to the results of Figure 5(a–e), through a change of the thickness of each of the three dielectric layers from $d = a/7 = 2.86$ mm to $d = a/8 = 2.5$ mm and by changing of ε_r from $\varepsilon_r = 10$ to $\varepsilon_{r1} = \varepsilon_{r3} = 8$, and $\varepsilon_{r2} = 9$. By changing only the radius of the cylinder, we can see from the results of Figures 5(a–e) and 6(a–e) that the field amplitude is greater when

Figure 6

The results for TE_{10} mode for four values of R: (a) $R = 53$ mm; (b) $R = 38$ mm; (c) $R = 29$ mm; and (d) $R = 27$ mm and for the periodic cross-section (Figure 1(c)). The other parameters are $d = a/8 = 2.5$ mm, $\varepsilon_{r1} = \varepsilon_{r3} = 8$, $\varepsilon_{r2} = 9$, $L_1 = a/4 = 5$ mm, $L_2 = a/2 = 10$ mm, and $L_3 = 3a/4 = 15$ mm; (e) the output field of the results (a)–(d) for $R = 53$ mm, $R = 38$ mm, $R = 29$ mm, and $R = 27$ mm, where $y = 0.5\ b$ and for the x-axis

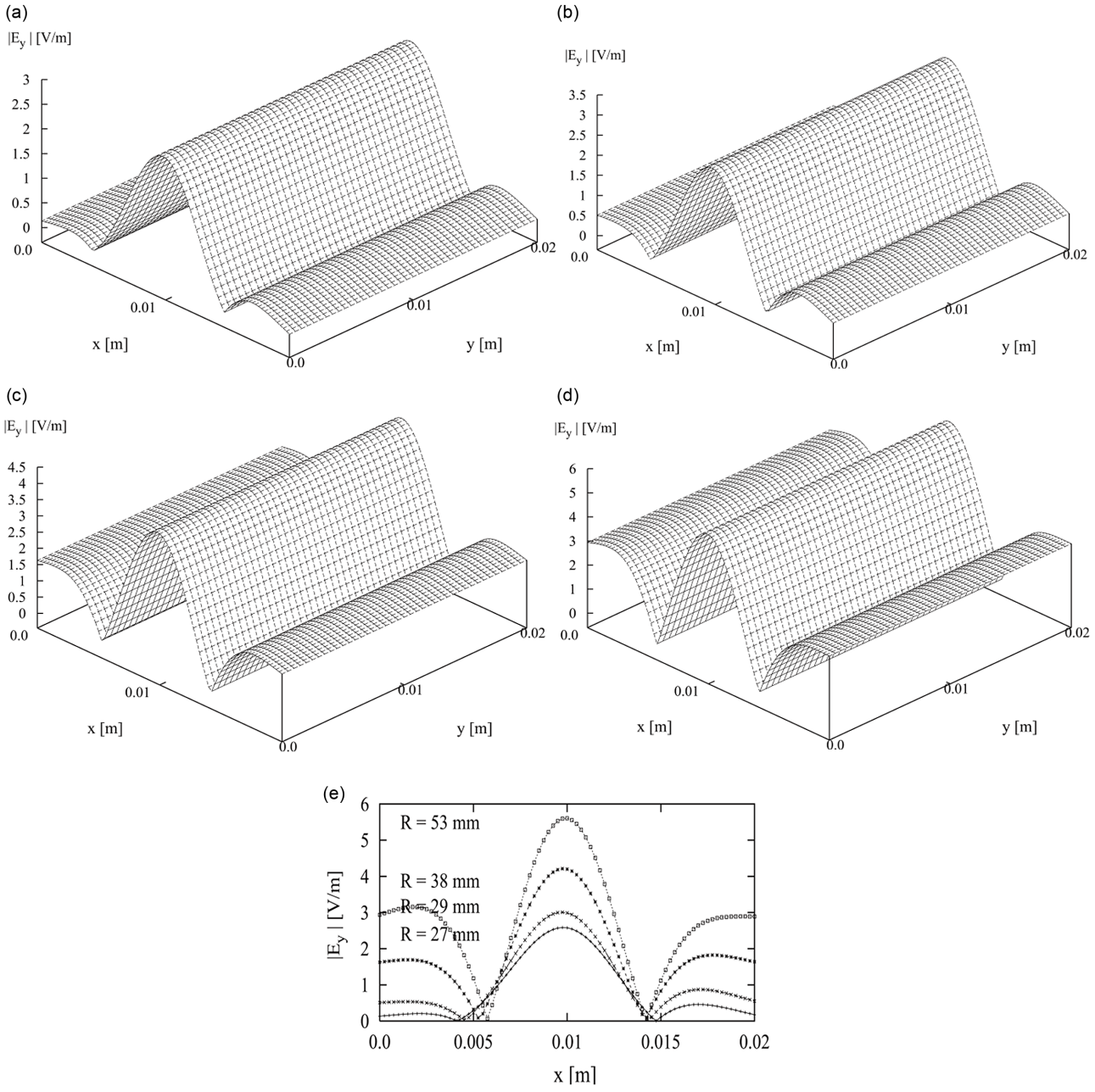

the radius of the cylinder is greater and that the width of the output profile is narrower.

5. Conclusions

The aim of this research was to examine the influence of curved waveguides with 7 alternating hollow and dielectric layers in the cross-section on the output field.

We generalized a previously published method [22] from a straight waveguide to both helical and toroidal waveguides for a specified periodic cross-section (Figure 1(c)). For this purpose, we used the method for curved waveguides [23] for the specific case of the periodic cross-section (Figure 1(c)).

The output field and the output power transmission are improved by increasing the δ_p or R, as demonstrated by numerical studies. The results of Figure 3 indicate that increasing the helix angle and the cylinder radius can lead to improve the output results of power transmission through the helical waveguide. Overall, the results of Figure 3 emphasize the significant impact of the helix angle and cylinder radius on the output power transmission.

By changing only the radius of the cylinder, we can see from the results of Figures 4(a–e) and 5(a–e) that the field amplitude is greater when the radius of the cylinder is greater and that the width of the output profile is narrower.

The results are true in the microwave and millimeter-wave regimes and can find utility in applications using a periodic array with alternating hollow and dielectric layers in a helical or toroidal waveguide. According to the logical results we get in the output profiles, we can determine what are the logical parameters that should be taken before any experiment in the laboratory that we want to perform.

Ethical Statement

This study does not contain any studies with human or animal subjects performed by the author.

Conflicts of Interest

The author declares that he has no conflicts of interest to this work.

Data Availability Statement

Data are available on request from the corresponding author upon reasonable request.

Author Contribution Statement

Zion Menachem: Conceptualization, Methodology, Software, Formal analysis, Investigation, Resources, Writing – original draft, Supervision.

References

[1] Marcatili, E. A. J., & Schmeltzer, R. A. (1964). Hollow metallic and dielectric waveguides for long distance optical transmission and lasers. *Bell System Technical Journal*, *43*(4), 1783–1809. https://doi.org/10.1002/j.1538-7305.1964.tb04108.x

[2] Marhic, M. E. (1981). Mode-coupling analysis of bending losses in IR metallic waveguides. *Applied Optics*, *20*(19), 3436–3441. https://doi.org/10.1364/AO.20.003436

[3] Miyagi, M., Harada, K., & Kawakami, S. (1984). Wave propagation and attenuation in the general class of circular hollow waveguides with uniform curvature. *IEEE Transactions on Microwave Theory and Techniques*, *32*(5), 513–521. https://doi.org/10.1109/TMTT.1984.1132715

[4] Wang, X., Yu, X., Berg, M. J., Chen, P., Lacroix, B., Fathpour, S., & Lei, S. (2021). Curved waveguides in silicon written by a shaped laser beam. *Optics Express*, *29*(10), 14201–14207. https://doi.org/10.1364/OE.419074

[5] Liu, W., Liu, H., Sun, X., & Zhang, F. (2023). The design of large curved waveguide based on sunflower graded photonic crystal. *Photonics*, *10*(7), 781. https://doi.org/10.3390/photonics10070781

[6] Qvotrup, C., Liu, Z., Papon, C., Wieck, A. D., Ludwig, A., & Midolo, L. (2024). Curved GaAs cantilever waveguides for the vertical coupling to photonic integrated circuits. *Optics Express*, *32*(3), 3723–3734. https://doi.org/10.1364/OE.510799

[7] Groth, E. B., Clarke, T. G. R., Schumacher da Silva, G., Iturrioz, I., & Lacidogna, G. (2020). The elastic wave propagation in rectangular waveguide structure: Determination of dispersion curves and their application in nondestructive techniques. *Applied Sciences*, *10*(12), 4401. https://doi.org/10.3390/app10124401

[8] Melloni, A., Monguzzi, P., Costa, R., & Martinelli, M. (2003). Design of curved waveguides: The matched bend. *Journal of the Optical Society of America A*, *20*(1), 130–137. https://doi.org/10.1364/JOSAA.20.000130

[9] Rosa, G. S. (2022). An accurate and numerically stable formulation for computing the electromagnetic fields in uniform bend rectangular waveguides. *IEEE Transactions on Microwave Theory and Techniques*, *71*(3), 988–996. https://doi.org/10.1109/TMTT.2022.3219830

[10] Krushynska, A. O., Anerao, N., Badillo-Ávila, M. A., Stokroos, M., & Acuautla, M. (2021). Arbitrary-curved waveguiding and broadband attenuation in additively manufactured lattice phononic media. *Materials & Design*, *205*, 109714. https://doi.org/10.1016/j.matdes.2021.109714

[11] Guennoc, T., Doc, J. B., & Félix, S. (2021). Improved multimodal formulation of the wave propagation in a 3D waveguide with varying cross-section and curvature. *The Journal of the Acoustical Society of America*, *149*(1), 476–486. https://doi.org/10.1121/10.0003336

[12] Zhang, S., Qin, L., Li, X., & Kube, C. M. (2020). Propagation of Rayleigh waves on curved surfaces. *Wave Motion*, *94*, 102517. https://doi.org/10.1016/j.wavemoti.2020.102517

[13] Liu, C., Zhou, J., Zhou, Y., Xu, L., & Chen, H. (2024). Broadband acoustic bend composed of homogeneous curved waveguides in quasi-two-dimensional space. *Applied Physics Letters*, *124*(8), 081702. https://doi.org/10.1063/5.0188393

[14] Sougleridis, I. I., Richoux, O., Achilleos, V., Theocharis, G., Desjouy, C., & Frantzeskakis, D. J. (2023). Acoustic solitons in a periodic waveguide: Theory and experiments. *Journal of Sound and Vibration*, *546*, 117433. https://doi.org/10.1016/j.jsv.2022.117433

[15] Wu, C. H., Qian, Z., Wang, W., Shen, J., Lin, X., Zheng, L. Y., . . . , & Zhang, H. (2023). A direct near-field observation of conversion between waveguide modes and leaky modes in periodic metal structures. *IEEE Access*, *11*, 16128–16141. https://doi.org/10.1109/ACCESS.2023.3244578

[16] Darche, M., Lopez-Caballero, F., & Tie, B. (2024). Modal analysis of waveguide for the study of frequency bandgaps of a bounded periodic medium. *Journal of Sound and Vibration*, *572*, 118158. https://doi.org/10.1016/j.jsv.2023.118158

[17] Tabatabaeian, Z. S., Kazemi, F., & Zarrabi, F. B. (2024). Periodic stub implementation with plasmonic waveguide as a slow-wave coupled cavity for optical refractive index sensing. *Scientific Reports*, *14*(1), 5175. https://doi.org/10.1038/s41598-024-55618-0

[18] Salem, M., Kirolous, H., & Abuelfadl, T. (2023). Analysis of periodic waveguide excitation with arbitrary shaped corrugation. In *40th National Radio Science Conference*, *1*, 62–73. https://doi.org/10.1109/NRSC58893.2023.10152981

[19] Abdrabou, A., & Lu, Y. Y. (2020). Complex modes in an open lossless periodic waveguide. *Optics Letters*, *45*(20), 5632–5635. https://doi.org/10.1364/OL.403204

[20] Ghahremani, M., & Shahabadi, M. (2023). Accurate characterization of complex Bloch modes in optical chain waveguides using real-valued computations. *Scientific Reports*, *13*(1), 22115. https://doi.org/10.1038/s41598-023-48477-8

[21] Menachem, Z., & Jerby, E. (1998). Transfer matrix function (TMF) for wave propagation in dielectric waveguides with arbitrary transverse profiles. *IEEE Transactions on Microwave Theory and Techniques*, *46*(7), 975–982. https://doi.org/10.1109/22.701451

[22] Menachem, Z. (2024). Propagation along the straight waveguide with a periodic array in the cross section and the behavior of the output fields. *Journal of Electrical and Electronics Engineering*, *19*(1), 15–27.

[23] Menachem, Z. (2022). Effective technique for analyzing rectangular helical and toroidal waveguides with a hollow rectangle bounded by dielectrical material and metal boundary. *Journal of Electromagnetic Waves and Applications*, *36*(6), 804–829. https://doi.org/10.1080/09205071.2021.1987336

[24] Vladimirov, V. S. (1971). *Equations of mathematical physics*. USA: Marcel Dekker.

[25] Salzer, H. E. (1955). Orthogonal polynomials arising in the numerical evaluation of inverse Laplace transforms. *Mathematics of Computation*, *9*(52), 164–177. https://doi.org/10.2307/2002053

[26] Salzer, H. E. (1961). Additional formulas and tables for orthogonal polynomials originating from inversion integrals. *Journal of Mathematics and Physics*, *40*(1–4), 72–86. https://doi.org/10.1002/sapm196140172

[27] Collin, R. E. (2007). *Foundations for microwave engineering*. USA: John Wiley & Sons.

How to Cite: Menachem, Z. (2025). The Output Field of Curved Waveguides with a Cross-Section of Alternating Hollow and Dielectric Layers. *Journal of Optics and Photonics Research*, *2*(2), 77–85. https://doi.org/10.47852/bonviewJOPR42023479

Appendix A

A comparison between our method and the analytical problem according to Collin [27] is shown in Figure 7(a) and according to the next equations.

$$E_y = \begin{cases} j\frac{k_z}{\varepsilon_0}\sin(vx) & 0 < x < t \\ j\frac{k_z}{\varepsilon_0}\frac{\sin(vt)}{\cos(\mu(t-a/2))}\cos(\mu(t-a/2))\cos[\mu(x-a/2)] & t < x < t+d \\ j\frac{k_z}{\varepsilon_0}\sin[v(a-x)] & t+d < x < a \end{cases}$$

where $v \equiv [k_o^2 - k_z^2]^{1/2}$ and $\mu \equiv [k_o^2 - k_z^2]^{1/2}$.

This is the input field at $z = 0$, where $a = 2$ cm, $b = 1$ cm, $d = 0.33$ cm, $t = 0.835$ cm, $c_r = 9$, and $\lambda = 6.9$ cm.

Our method is dependent on the number of the modes in the system. The order ($N = 1,3,5,7,$ and 9) increases, and we show from Figure 7(b) that $E_y(N = 9)$ approaches the result E_y of the analytical solution [27]. The comparison gives us good agreement.

Figure 7
(a) A cross-section for the straight waveguide and
(b) the result between our model and theoretical model